ACS OMEGA

http://pubs.acs.org/journal/acsodf

Article

# Niobium K-Edge X-ray Absorption Spectroscopy of Doped $TiO_2$ Produced from Ilmenite Digested in Hydrochloric Acid

Richard G. Haverkamp,* Peter Kappen, Katie H. Sizeland, and Kia S. Wallwork

Cite This: *ACS Omega* 2022, 7, 28258−28264

Read Online

ACCESS | Metrics & More | Article Recommendations | Supporting Information

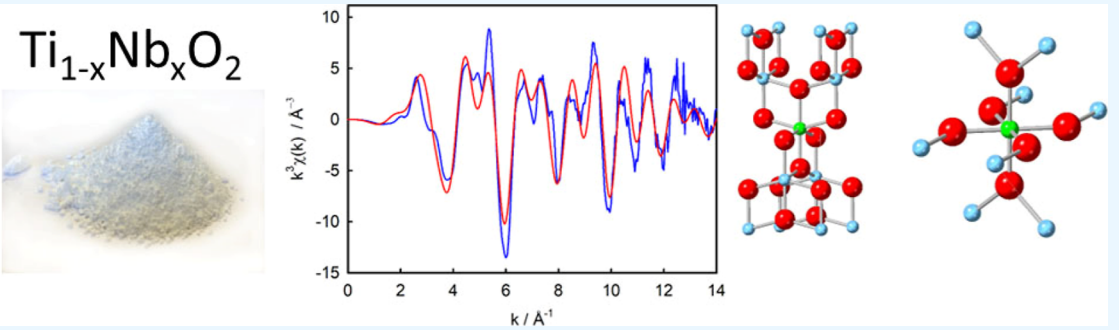


**ABSTRACT:** Niobium doping of $TiO_2$ creates a conductive material with many new energy applications. When $TiO_2$ is precipitated from HCl solutions containing minor Nb, the Nb in solution is quantitatively deposited with the $TiO_2$. Here, we investigate the structure of Nb doped in anatase and rutile produced from ilmenite digested in hydrochloric acid. Nb K-edge X-ray absorption near edge structure (XANES) and extended X-ray absorption fine structure (EXAFS) are used to characterize the environment of 0.08 atom % Nb doped in $TiO_2$. XANES shows clear structural differences between Nb-doped anatase and rutile. EXAFS for Nb demonstrates that Nb occupies a Ti site in $TiO_2$ with no near neighbors of Nb. Hydrolysis of Ti and Nb from acid solution, followed by calcination, leads to a well dispersed doped material, with no segregation of Nb. Production of Nb-doped $TiO_2$ by this method may be able to supply future demand for large quantities of the material and in energy applications where a low cost of production, from readily available natural resources, would be highly desirable.



## 1. INTRODUCTION

The dominant use of $TiO_2$ is for the white pigment.[1] However, many non-pigment applications of $TiO_2$ have been developed or are being considered. One important feature of $TiO_2$ that enables new applications is the ability to modify this normally insulating material to become an electrical conductor. One way to produce this conductivity is by doping of $TiO_2$ with niobium. If these applications are to become economical, a means to produce Nb-doped $TiO_2$ on an industrial scale is required.

A proposed production method for $TiO_2$ from the relatively abundant titanium containing ore, ilmenite, is the digestion in HCl[2] and subsequent precipitation of a titanium oxide hydrate directly from solution,[3] followed by calcination. In this process, Nb naturally present in the ilmenite dissolves and is quantitatively precipitated with the $TiO_2$. Either rutile or anatase forms can be made directly or anatase formed and converted into rutile by calcination.

Nb-doped $TiO_2$ can act similar to a transparent metal which could be used in the place of indium-tin-oxide (Sn-doped $In_2O_3$), which is widely used in flat panel displays, touch panels, and light-emitting devices.[4] Other uses for Nb-doped $TiO_2$ include photovoltaics[5] and dye-sensitized solar cells.[6−8] It also finds application in photocatalysis[9] including for the production of $H_2$,[10] photoelectrochemical water splitting,[11] and photocatalytic $CO_2$ reduction.[12] Other catalytic applications are for catalyst supports,[13] for example, for the oxygen reduction reaction[14] and $H_2$ production,[15] or for dimensionally stable anodes for the chlorine evolution reaction,[16] and electrochemical destruction of "forever chemicals".[17] Nb-doped $TiO_2$ has potential application in batteries and supercapacitors[18] including lithium-ion batteries[19,20] and Na-ion batteries.[21] Other potentials uses are for CO sensing[22] and thermoelectric power production.[23]

These many possible uses of Nb-doped $TiO_2$, many of which are in new energy developments, suggest that there could be future demand for large quantities of the material and in applications where a low cost of production would be required.

**Received:** April 29, 2022
**Accepted:** July 22, 2022
**Published:** August 4, 2022

Therefore, a process to produce the doped material on a large scale from readily available natural resources is highly desirable.

For doping of $TiO_2$ to display modified electronic properties, it may be necessary for the dopant to be distributed throughout the material. Therefore, any method for the bulk production of doped $TiO_2$ should also evaluate the nature of the incorporation of the dopant.

In this work, the nature of the incorporation of Nb into $TiO_2$ produced from hydrolysis of HCl solutions of Barrytown, New Zealand ilmenite is investigated. X-ray absorption near edge structure (XANES) and extended X-ray absorption fine structure (EXAFS), supported by X-ray diffraction (XRD), are used to characterize the local environment of Nb in both anatase and rutile phases of $TiO_2$. The purpose is to determine whether Nb occupies Ti sites without significantly modifying the $TiO_2$ structure or if Nb is intermixed as a distinct oxide phase.

## 2. EXPERIMENTAL SECTION

**2.1. Preparation of $TiO_2$.** Placer ilmenite from Barrytown, New Zealand, containing 0.05% $Nb_2O_5$, was digested in 35 wt % hydrochloric acid and precipitated as $TiO_2$ hydrate with either rutile or anatase structure, as described in more detail elsewhere.[3] Rutile hydrate is the natural product from the hydrolysis of HCl solutions, while the anatase hydrate was obtained by the addition of $H_3PO_4$ in the seeding stage of the hydrolysis (equivalent to 0.35% $P_2O_5$ in the final $TiO_2$ product). The hydrate, after the addition of KCl to the level of 0.3% $K_2O$, was calcined at 925 °C for 1 h, thus yielding the $TiO_2$ material used in this study.

**2.2. Elemental Analysis.** The elemental composition of the titanium dioxide hydrates,[3] prior to calcination, were determined by Spectrachem Analytical Services, Lower Hutt, New Zealand. The analyses were performed on a Siemens SRS303AS wavelength-dispersive X-ray fluorescence spectrometer. Pressed powder samples were used with the Siemens "Spectraplus" semi-quantitative multi-element analysis.

**2.3. X-ray Diffraction.** XRD was performed at the bending magnet powder diffraction beamline at the Australian Synchrotron. This beamline uses a Mythen II silicon microstrip detector with an intrinsic angular resolution of 0.004°.[24] For the experiments, the wavelength was set at $\lambda$ = 0.58959 (1) Å ($E$ = 21 keV), and the vertical beam size was 0.4−0.5 mm at the sample. Samples were packed in 0.3 mm quartz capillaries, with 0.01 mm wall thickness (W. Müller, Schönwalde). The wavelength was determined accurately through Rietveld analysis of the diffraction pattern from $LaB_6$.

**2.4. X-ray Absorption Spectroscopy.** X-ray absorption spectroscopy (XAS) was performed at the wiggler XAS beamline at the Australian Synchrotron. Samples were finely ground with a mortar and pestle and pressed into pellets. Spectra across the Nb K-edge ($E_0$ = 18,985.6 eV[25]) were recorded in the fluorescence mode with a 100-element detector (Canberra). The samples were held in a He-cooled cryostat ($T$ < 20 K). Energy steps of 10 eV pre-edge and 0.35 eV across the edge (1 s/step) were used. In the EXAFS range, $k$-steps of 0.035 $Å^{-1}$ (up to 5 s/step) were used. The energy scale was calibrated by simultaneously measuring a Nb foil placed between the two downstream ion chambers. The photon flux at the sample was around $10^{10}$ photons $s^{-1}$. No signs of radiation damage were detected from repeat scans, permitting multiple scans to be summed in order to improve signal-to-noise. Reference standards were Nb foil as well as 0.02% $NbO_2$ (Aldrich) and $Nb_2O_5$ (Aldrich) both diluted to 0.02% in boric acid and loaded into 1 mm thick sample holders. The beam size at the sample was about 1.5 × 0.4 mm ($H \times V$).

XANES and EXAFS data were processed using the freeware package Athena/Artemis,[26] with scattering paths provided through FEFF6.[27]

## 3. RESULTS AND DISCUSSION

**3.1. X-ray Diffraction.** The two samples of $TiO_2$ prepared for this study are shown to be highly crystalline anatase or rutile (Figure 1) with no detectable admixture of the two phases in either sample and no other phases present.

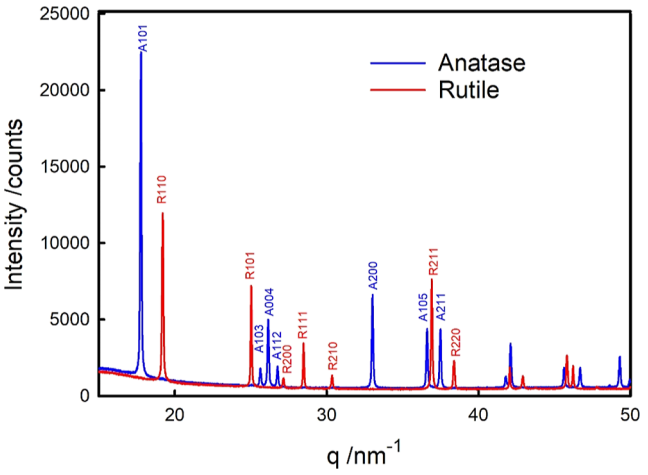


**Figure 1.** X-ray diffraction patterns of Nb-doped anatase (blue) and Nb-doped rutile (red) with the peaks identified by their Miller indices (and indicated A for an anatase diffraction, R for a rutile diffraction).

**3.2. Elemental Composition.** The $TiO_2$ hydrates that were the basis for the anatase and rutile materials used in this work both contained Nb at the level of 0.13% "$Nb_2O_5$" (see Table 1, taken from ref 3); this oxide represents the conventional method to convey elemental concentrations and does not mean the oxide must be in this form. The reported concentration corresponds to 0.08 atom % Nb of the Ti + Nb. These also contain phosphorous, a portion of which comes from inclusions in the ilmenite ore[28] and with additional phosphorous added to produce anatase instead of the naturally

**Table 1. Elemental Composition of the Two $TiO_2$ Materials Prior to Calcination**[a]

| element as oxide | anatase wt % | rutile wt % |
|---|---|---|
| $TiO_2$ | 94.3 | 95.8 |
| $P_2O_5$ | 0.82 | 0.49 |
| $Nb_2O_5$ | 0.13 | 0.13 |
| $Ta_2O_5$ | 0.009 | 0.009 |
| Cl | 4.4 | 3.1 |
| FeO | 0.015 | 0.044 |
| $SiO_2$ | 0.19 | 0.28 |
| $Al_2O_3$ | 0.07 | 0.03 |
| CaO | 0.01 | 0.02 |
| $K_2O$ | 0.006 | 0.01 |

[a]Reprinted with permission from Haverkamp, R. G.; Wallwork, K.; Waterland, M.; Gu, Q.; Kimpton, J. A. *Ind. Eng. Chem. Res.* **2022,** *61* (19), 6333−634. Copyright 2022 American Chemical Society.[3]



https://doi.org/10.1021/acsomega.2c02676
*ACS Omega* 2022, 7, 28258−28264

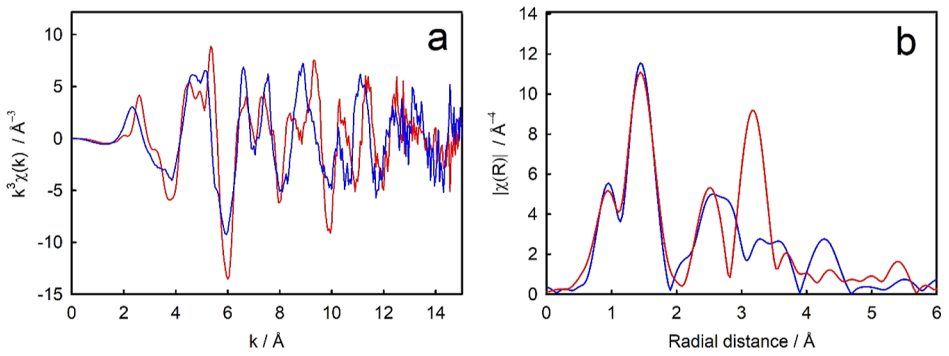


**Figure 2.** Nb K-edge XANES of Nb-doped $TiO_2$ (anatase and rutile) and Nb oxide standards (offset by +0.3).

formed rutile. Si, Al, Ca, and K (except the K added later as a calcination flux) are likely to be present as discrete finely divided gangue material, from inclusions in the ilmenite ore, that passed through filtration steps and became incorporated in the hydrolysis product and subsequently in the calcined material. This work did not specifically ascertain the form of the Si, Al, Ca, and K, but as the solubility of these materials is low in hydrochloric acid used for the ore digestion. Small inclusions of minerals such as garnet and feldspar are typically present in ilmenite, thus posing a likely route to the inclusion of these elements in the rutile and anatase precipitates.

**3.3. X-ray Absorption Near Edge Structure.** The primary purpose of this work is to determine the nature of the Nb present in the $TiO_2$ of the two different structures. XANES can be used to compare materials of interest with reference materials, primarily providing chemical information. Here, we compare the Nb-doped anatase with the Nb-doped rutile and with two niobium oxide reference compounds. There are clear differences in the Nb K-edge XANES between the Nb-rutile and the Nb-anatase forms (Figure 2). The edge energy is the same in both Nb-doped anatase and rutile (at ~18,988 eV). However, there are significant differences above the absorption edge, both in the whiteline and further into the XANES region. The reference compounds (Figure 2) contain Nb in $NbO_2$ with oxidation state 4+ and $Nb_2O_5$ with oxidation state 5+. The $Nb_2O_5$ has an edge energy of 19,000.2 eV which is similar to that of the Nb-doped $TiO_2$ materials and also contains a pre-edge feature similar to that present in those doped materials. The $NbO_2$ has a lower edge energy of 18,997.7 eV than $Nb_2O_5$, reflecting the lower oxidation state of $NbO_2$. The edge for the Nb metal at 18985.6 eV lies at a lower energy than these oxides.[25] From the XANES, it is therefore apparent that Nb in the doped anatase and rutile has a different chemical/structural environment in each of the two forms. A published XANES study of 7 atom % Nb doping in anatase $TiO_2$ presents a similar spectrum to the 0.08 atom % Nb-doped $TiO_2$ here for the anatase form.[9] XANES of 1.5% Nb in anatase $TiO_2$ has also recently been published, where ab initio finite difference method near edge structure using the density functional theory simulation was used to model the spectrum providing good agreement between the data and the model of Nb in anatase.[29]

**3.4. Extended X-ray Absorption Fine Structure.** The Nb K-edge EXAFS of the doped anatase and rutile produced markedly different spectra. The Fourier transforms of these spectra, plotted as radial distance versus the magnitude of the Fourier transform (Figure 3), show that the structural environments of Nb in these two materials are quite different.

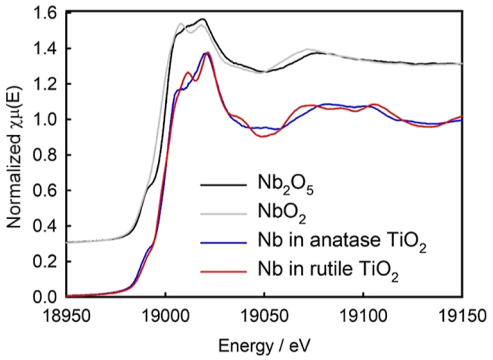


**Figure 3.** Comparison of recorded spectra for Nb K-edge EXAFS of Nb-doped anatase (blue) and Nb-doped rutile (red) $TiO_2$. (a) $k^3$, (b) Fourier transform.

The EXAFS was therefore analyzed by solving the EXAFS equation for crystal structures that might be present and comparing these with the experimental data using the following procedure.

$TiO_2$ structures were obtained from the Crystallography Open Database[30] for anatase and rutile, as well as a wide range of niobium oxide structures. For the oxides, structure models were loaded into *Artemis* as is. For Nb-doped $TiO_2$ structures, the *Atoms* routine in *Artemis* was run with Nb set as the absorber in place of Ti; scattering paths and phases were then calculated using FEFF. Due to the low concentration of Nb, it was assumed that Nb was isolated on the scale of the attenuation length of electrons in the structure. This assumption was tested against experimental data by fitting. Anatase and rutile structures (with Nb substituted) were evaluated, as were a wide variety of $Nb_2O_5$ and $NbO_2$ structures. None of the niobium oxide structures gave good fits, and these attempted fits are provided in the Supporting Information.

Fitting of the structures to the EXAFS data was performed in real space ($R$), with the quality of fit parameters shown in Table 2. Fairly good fits were obtained, with a fit to a Nb substituted for Ti in anatase and a Nb substituted for Ti in rutile matching well to the experimental data for the Nb-doped anatase and rutile samples, respectively (Figure 4). These unconstrained fits gave $S_0^2$ close to 1 in both cases ($1.05 \pm 0.23$ and $1.06 \pm 0.14$) which provides good confidence that the fitted model in each case is appropriate.

The EXAFS fit reveals that Nb is substituted into Ti sites of the crystal structure adopted in each case, anatase or rutile, as represented in the structures shown in Figure 5. The Nb is well dispersed and does not appreciably interact with other Nb


https://doi.org/10.1021/acsomega.2c02676
ACS Omega 2022, 7, 28258−28264

**Table 2. EXAFS Structure Fitting Conditions and Quality of Fit Parameters**

| sample | structure fitted (CIF file) | data range used, $k$ (Å$^{-1}$) | fitting range in $R$ (Å) | reduced $\chi^2$ | $R$ factor | $S_0^2$ (error) | $\Delta R$ | $\sigma^2$ (Debye–Waller) |
|---|---|---|---|---|---|---|---|---|
| Nb-doped anatase | 1010942 anatase[31] | 2–11.5 | 1.01–6 | 99 | 0.19 | 1.05 (0.22) | 0.068 | 0.0058 |
| Nb-doped rutile | 9004141 rutile[32] | 2–14 | 1.01–6 | 35 | 0.16 | 1.06 (0.14) | 0.048 | 0.0067 |

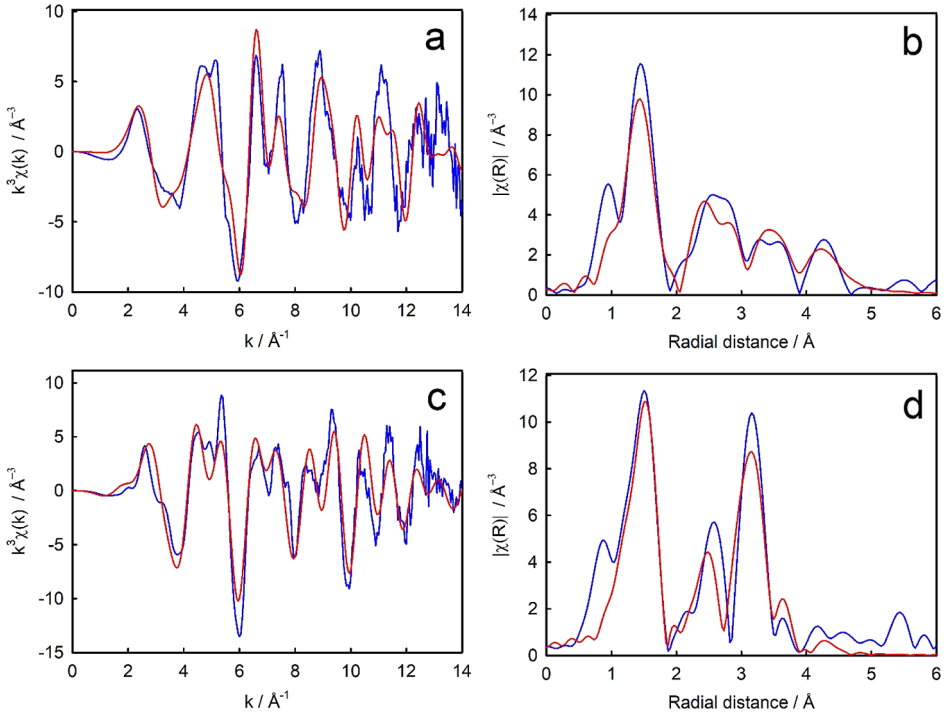


**Figure 4.** Nb K-edge EXAFS structure fits to data for Nb substituted in a Ti site in *k*-space and *R*-space; (a,b) anatase; and (c,d) rutile. Recorded spectra are shown in blue and *Artemis* fits to the data for the best fit crystal structures are shown in red.

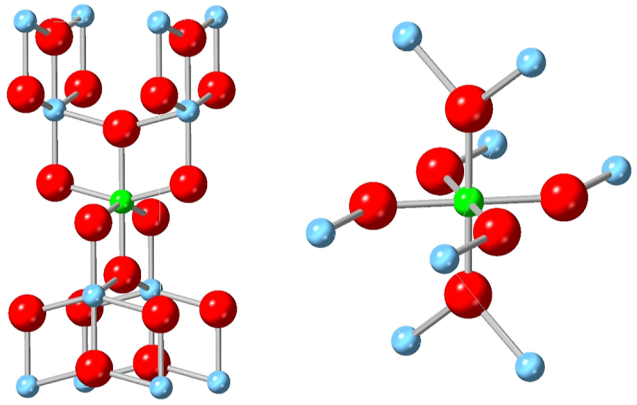

**Figure 5.** Crystal structures with Nb in anatase (left) and Nb in rutile (right). Green, Nb; blue, Ti; red, O. Generated using CrystalDiffract, CrystalMaker Software Ltd, Oxford, England (www.crystalmaker.com).

atoms in the structure, and it is not present as niobium oxide clusters within $TiO_2$ of clusters separate to $TiO_2$, consistent with the XANES data discussed above. The EXAFS results also indicate that it is unlikely that Nb forms dimers as has been postulated in some Nb-doped $TiO_2$.[33] In other studies, anatase thin films were prepared from a composite TiNb target by reactive magnetron sputtering giving a level of 1.5% Nb doped in $TiO_2$ anatase.[29] The authors conclude that "the local environment of Nb atoms in the film is close to that of Ti atoms in the anatase phase [...]. This suggests that the substitution of Ti by Nb ions occurs in the film without a strong influence on the $TiO_2$ matrix". Here, we come to a similar conclusion for these bulk materials formed by hydrolysis and with both anatase and rutile where the Nb takes Ti sites in either structure without appreciably modifying the structure. However, it is noted that in other work with $TiO_2$ doped to 2.9 atom % Nb or higher, there was a phase change from anatase to rutile on calcination the Nb was segregated, leading to the formation of NbO nanoclusters on the surface of the $TiO_2$ rutile nanoparticles even before the phase change took place.[34] In the work described here, we see no segregation of Nb in the calcined material, with the data supporting highly dispersed Nb substituting for Ti in $TiO_2$ structures. This is a positive consideration for energy applications of this material, as discussed further below (Section 3.7).

**3.5. Industrial Production of Nb-Doped $TiO_2$.** If the many potential applications of Nb-doped $TiO_2$ are to be realized, a low-cost and scalable method to produce such a material is highly desirable. Ilmenite is the main primary source of $TiO_2$ and sometimes also contains niobium. The Barrytown, New Zealand ilmenite used here is from a large placer deposit and has an average concentration of 0.05% $Nb_2O_5$ (350 ppm Nb) in the bulk ilmenite with 200–800 ppm Nb in individual ilmenite grains.[28] It is one potential source for the large-scale production of Nb-doped $TiO_2$ materials and has been shown to be amenable to this hydrothermal method both being highly soluble in HCl[2] and readily precipitated[3] and calcined to form either anatase or rutile. This process is similar to the "sulfate


https://doi.org/10.1021/acsomega.2c02676
ACS Omega 2022, 7, 28258–28264

process" for the large-scale production of pigment grade $TiO_2$ which uses sulfuric acid rather than hydrochloric acid.

Other ilmenite deposits have also been reported to contain Nb at useful levels. A West Australian sand deposit contains 1000 ppm Nb on average with up to 3500 ppm Nb in some mineral grains.[35] Ilmenite from Richard's Bay, South Africa, contains 460 ppm Nb.[36] An ilmenite sand deposit, at Walikale, North Kivu, Democratic Republic of Congo, contains 157 ppm Nb on average with 40−341 ppm Nb in individual grains.[37] An ilmenite deposit in Kuru town, Jos South, Plateau State, Nigeria may have up to 4.4% Nb.[38] Some of these deposits may be suitable for this process; however, only some ilmenites are readily soluble in hydrochloric acid and other elements present in these ores may also contribute either favorably or unfavorably to the product formed.

The Nb doping level could be increased by the addition of extra Nb, either by concentration from the digestion solutions, adding a soluble Nb ore to the digestion process, or by the addition of a suitable Nb salt to the digestion liquor prior to hydrolysis. The XANES and EXAFS presented here have demonstrated that the Nb is incorporated into the lattice of $TiO_2$ by this preparation method.

Production of Nb-doped $TiO_2$ has been proposed by sol−gel synthesis, for example, for anatase beads with 0.1−10 atom % Nb from starting material of titanium(IV) isopropoxide with 1-hexadecylamine as a structure-directing agent for use in Li-ion batteries.[20] A similar sol−gel synthesis of $TiO_2$ doped with about 10% Nb from titanium tetrabutyl titanate with 1-hexadecylamine and polydimethylsiloxane as structure determining agents was prepared for use in electrorheological fluids.[39] A sol−gel preparation followed by spark plasma sintering with repeated oxidation and reduction is another method proposed for the preparation of Nb-doped $TiO_2$ powders.[33] Another possible synthesis route is by grinding precursors of $TiNb_2O_7$ and $TiO_2$ in a mechanochemical synthesis[15] which results in a mixture with a gradient in Nb concentration with more Nb on the surface. However, for large-scale production, preparation by the hydrolysis of aqueous acid solutions to form $TiO_2$ is well established on an industrial scale and therefore readily adaptable to produce Nb-doped material.

**3.6. Other Effects of Nb on $TiO_2$ Production.** The action of doping $TiO_2$ with Nb at hydrolysis to produce a material suitable for the many proposed applications may lead to changes to other properties of the material. The anatase to rutile phase change may be retarded by increased Nb doping[34,40−44] which may be desirable in some circumstances (when anatase in the desired end product) but undesirable in other circumstances (e.g., more flux may be required to produce rutile from anatase at a suitably small particle size). Final product color may be influenced by the presence of Nb, giving a blue tint. However, this color change is often desirable for pigments and can counteract a yellow tint produced by iron or some other impurities.[9,43,45,46]

**3.7. Why the Placement of Nb is Important for the Electrical and Optical Properties.** It has been shown here that Nb doped into $TiO_2$ substitutes in the Ti site for either anatase or rutile and can therefore be fully dispersed within the $TiO_2$ material. It is important that Nb does this, rather than forming discrete clusters, in order for the electronic, optical, and photocatalytic properties to be realized.

The electrical conductivity of Nb-doped $TiO_2$ depends on both the level of Nb doping with the conductivity increasing approximately linearly with Nb content over the range 0.003−0.03 atom % Nb.[47] The electrical conductivity is also dependent on the number of oxygen vacancies. The Nb(V) substituting for Ti(IV) requires a charge balance which is met by oxygen deficiency. However, oxygen deficiency can also result from the reducing conditions in the treatment of the Nb-doped $TiO_2$. Under mildly reducing conditions (in a study of 0.65 atom % Nb in $TiO_2$), an n-type semiconductor is formed, whereas under strongly reducing conditions metallic charge transport is developed.[48] A density functional theory calculation (screened exchange hybrid functional method) showed that shallow conduction bands should be present in Nb-doped anatase $TiO_2$, but deep conduction bands in rutile $TiO_2$.[49] The calculations suggested that Nb donors are compensated by interstitial oxygen anions except at low oxygen partial pressures and low O pressures prevent O interstitials being formed rather than create extra O vacancies. If too much O is removed, the material is no longer transparent as a thin film.[49]

We therefore might expect the Nb-doped rutile form produced in the work presented here to be less electrically conductive than the Nb-doped anatase form, when compared in similar oxygen partial pressure environments. We have shown that the Nb is placed in the Ti sites rather than as dimers or a discrete phase and this enables the electronic properties of the doped material to be realized.

## 4. CONCLUSIONS

Niobium-doped $TiO_2$, at a level of 0.08 atom % Nb, was produced by the hydrolysis of liquor from the digestion of ilmenite in hydrochloric acid as either anatase or rutile and calcined to form Nb-doped anatase or rutile. XANES of these doped materials showed that Nb in the doped anatase and rutile has a different chemical/structural environment in each of the two forms and the Nb is not in the form of a previously known Nb oxide structure. An EXAFS analysis revealed that Nb is substituted into Ti sites of the crystal structure adopted in each case, anatase or rutile, and that Nb is well dispersed and does not appreciably interact with other Nb atoms in the structure and is not present as niobium oxide clusters within $TiO_2$. Segregation of Nb did not occur on calcination. This placement of Nb in Ti sites, well dispersed, is important in order for the electronic, optical, and photocatalytic properties to be realized. Because this method produces Nb substituted into Ti sites and because it is analogous to current industrial scale $TiO_2$ production methods, it may be a suitable low cost method of producing Nb-doped material to realize the many potential applications of Nb-doped $TiO_2$, especially if Nb levels are boosted by the addition of Nb to the hydrolysis solution..

## ■ ASSOCIATED CONTENT

### Supporting Information

The Supporting Information is available free of charge at https://pubs.acs.org/doi/10.1021/acsomega.2c02676.

EXAFS attempted fits of structures that are not a good match to the data (PDF)

## ■ AUTHOR INFORMATION

### Corresponding Author

**Richard G. Haverkamp** − *School of Engineering and Advanced Technology, Massey University, Palmerston North*



https://doi.org/10.1021/acsomega.2c02676
ACS Omega 2022, 7, 28258−28264

*4442, New Zealand;* orcid.org/0000-0002-3890-7105; Email: r.haverkamp@massey.ac.nz

### Authors

**Peter Kappen** − *Australian Synchrotron, ANSTO, Clayton 3168 Victoria, Australia*

**Katie H. Sizeland** − *Australian Synchrotron, ANSTO, Clayton 3168 Victoria, Australia*

**Kia S. Wallwork** − *Australian Synchrotron, ANSTO, Clayton 3168 Victoria, Australia*

Complete contact information is available at: https://pubs.acs.org/10.1021/acsomega.2c02676

### Notes

The authors declare no competing financial interest.

## ■ ACKNOWLEDGMENTS

This research was undertaken on the XAS and PD Beamlines at the Australian Synchrotron, part of the ANSTO; grant numbers M4871 and M2870. Travel funding was provided by the New Zealand Synchrotron Group.

## ■ REFERENCES

(1) Gambogi, J. *Titanium and titanium dioxide. Mineral Commodity Summaries*; U.S. Geological Survey: Reston, VA, 2021. https://pubs.usgs.gov/periodicals/mcs2021/mcs2021-titanium.pdf.

(2) Haverkamp, R. G.; Kruger, D.; Rajashekar, R. The digestion of New Zealand ilmenite by hydrochloric acid. *Hydrometallurgy* **2016**, *163*, 198−203.

(3) Haverkamp, R. G.; Wallwork, K.; Waterland, M.; Gu, Q.; Kimpton, J. A. Controlled hydrolysis of TiO2 from HCl digestion liquors of ilmenite. *Ind. Eng. Chem. Res.* **2022**, *61*, 6333−6342.

(4) Furubayashi, Y.; Hitosugi, T.; Yamamoto, Y.; Inaba, K.; Kinoda, G.; Hirose, Y.; Shimada, T.; Hasegawa, T. A transparent metal: Nb-doped anatase $TiO_2$. *Appl. Phys. Lett.* **2005**, *86*, 252101.

(5) Potlog, T.; Dumitriu, P.; Dobromir, M.; Manole, A.; Luca, D. Nb-doped $TiO_2$ thin films for photovoltaic applications. *Mater. Des.* **2015**, *85*, 558−563.

(6) Nikolay, T.; Larina, L.; Shevaleevskiy, O.; Ahn, B. T. Electronic structure study of lightly Nb-doped $TiO_2$ electrode for dye-sensitized solar cells. *Energy Environ. Sci.* **2011**, *4*, 1480−1486.

(7) Su, H.; Huang, Y. T.; Chang, Y. H.; Zhai, P.; Hau, N. Y.; Cheung, P. C. H.; Yeh, W. T.; Wei, T. C.; Feng, S. P. The Synthesis of Nb-doped $TiO_2$ Nanoparticles for Improved-Performance Dye Sensitized Solar Cells. *Electrochim. Acta* **2015**, *182*, 230−237.

(8) Kavan, L.; Grätzel, M.; Gilbert, S. E.; Klemenz, C.; Scheel, H. J. Electrochemical and photoelectrochemical investigation of single-crystal anatase. *J. Am. Chem. Soc.* **1996**, *118*, 6716−6723.

(9) Bhachu, D. S.; Sathasivam, S.; Sankar, G.; Scanlon, D. O.; Cibin, G.; Carmalt, C. J.; Parkin, I. P.; Watson, G. W.; Bawaked, S. M.; Obaid, A. Y.; et al. Solution processing route to multifunctional titania thin films: Highly conductive and photcatalytically active Nb:$TiO_2$. *Adv. Funct. Mater.* **2014**, *24*, 5075−5085.

(10) Caudillo-Flores, U.; Muñoz-Batista, M. J.; Kubacka, A.; Fernández-García, M. Pd-Pt bimetallic Nb-doped $TiO_2$ for $H_2$ photo-production: Gas and liquid phase processes. *Mol. Catal.* **2020**, *481*, 110240.

(11) Das, C.; Roy, P.; Yang, M.; Jha, H.; Schmuki, P. Nb doped $TiO_2$ nanotubes for enhanced photoelectrochemical water-splitting. *Nanoscale* **2011**, *3*, 3094−3096.

(12) Huang, J.; Lv, T.; Huang, Q.; Deng, Z.; Chen, J.; Liu, Z.; Wang, G. Effect of Rh valence state and doping concentration on the structure and photocatalytic $H_2$ evolution in (Nb, Rh) codoped $TiO_2$ nanorods. *Nanoscale* **2020**, *12*, 22082−22090.

(13) Park, K. W.; Seol, K. S. Nb-$TiO_2$ supported Pt cathode catalyst for polymer electrolyte membrane fuel cells. *Electrochem. Commun.* **2007**, *9*, 2256−2260.

(14) Hussain, S.; Erikson, H.; Kongi, N.; Tarre, A.; Ritslaid, P.; Kikas, A.; Kisand, V.; Kozlova, J.; Aarik, J.; Tamm, A.; Sammelselg, V.; Tammeveski, K. Platinum sputtered on Nb-doped $TiO_2$ films prepared by ALD: highly active and durable carbon-free ORR electrocatalyst. *J. Electrochem. Soc.* **2020**, *167*, 164505.

(15) Tarutani, N.; Kato, R.; Uchikoshi, T.; Ishigaki, T. Spontaneously formed gradient chemical compositional structures of niobium doped titanium dioxide nanoparticles enhance ultraviolet- and visible-light photocatalytic performance. *Sci. Rep.* **2021**, *11*, 15236.

(16) Lim, H. W.; Cho, D. K.; Park, J. H.; Ji, S. G.; Ahn, Y. J.; Kim, J. Y.; Lee, C. W. Rational design of dimensionally stable anodes for active chlorine generation. *ACS Catal.* **2021**, *11*, 12423−12432.

(17) Ko, J. S.; Le, N. Q.; Schlesinger, D. R.; Johnson, J. K.; Xia, Z. Novel niobium-doped titanium oxide towards electrochemical destruction of forever chemicals. *Sci. Rep.* **2021**, *11*, 18020.

(18) Lindberg, S.; Cavallo, C.; Calcagno, G.; Navarro-Suárez, A. M.; Johansson, P.; Matic, A. Electrochemical Behaviour of Nb-Doped Anatase $TiO_2$ Microbeads in an Ionic Liquid Electrolyte. *Batteries Supercaps* **2020**, *3*, 1233−1238.

(19) Xu, W.; Russo, P. A.; Schultz, T.; Koch, N.; Pinna, N. Niobium-Doped Titanium Dioxide with High Dopant Contents for Enhanced Lithium-Ion Storage. *ChemElectroChem* **2020**, *7*, 4016−4023.

(20) Cavallo, C.; Calcagno, G.; de Carvalho, R. P.; Sadd, M.; Gonano, B.; Araujo, C. M.; Palmqvist, A. E.; Matic, A. Effect of the Niobium Doping Concentration on the Charge Storage Mechanism of Mesoporous Anatase Beads as an Anode for High-Rate Li-Ion Batteries. *ACS Appl. Energy Mater.* **2020**, *4*, 215−225.

(21) Usui, H.; Yoshioka, S.; Wasada, K.; Shimizu, M.; Sakaguchi, H. Nb-doped rutile $TiO_2$: A potential anode material for Na-ion battery. *ACS Appl. Mater. Interfaces* **2015**, *7*, 6567−6573.

(22) Duta, M.; Predoana, L.; Calderon-Moreno, J. M.; Preda, S.; Anastasescu, M.; Marin, A.; Dascalu, I.; Chesler, P.; Hornoiu, C.; Zaharescu, M.; et al. Nb-doped $TiO_2$ sol-gel films for CO sensing applications. *Mater. Sci. Semicond. Process.* **2016**, *42*, 397−404.

(23) Ribeiro, J.; Correia, F.; Rodrigues, F.; Reparaz, J.; Goñi, A.; Tavares, C. Transparent niobium-doped titanium dioxide thin films with high Seebeck coefficient for thermoelectric applications. *Surf. Coat. Technol.* **2021**, *425*, 127724.

(24) Wallwork, K. S.; Kennedy, B. J.; Wang, D. The high resolution powder diffraction beamline for the Australian Synchrotron. In *AIP Conference Proceedings*; Wallwork, K. S., Kennedy, B. J., Wang, D., Eds., 2007; Vol. *879*, pp 879−882.

(25) Sasaki, K.; Zhang, L.; Adzic, R. R. Niobium oxide-supported platinum ultra-low amount electrocatalysts for oxygen reduction. *Phys. Chem. Chem. Phys.* **2008**, *10*, 159−167.

(26) Ravel, B.; Newville, M. ATHENA,ARTEMIS,HEPHAESTUS: data analysis for X-ray absorption spectroscopy usingIFEFFIT. *J. Synchrotron Radiat.* **2005**, *12*, 537−541.

(27) Zabinsky, S.; Rehr, J.; Ankudinov, A.; Albers, R.; Eller, M. Multiple-scattering calculations of X-ray-absorption spectra. *Phys. Rev. B: Condens. Matter Mater. Phys.* **1995**, *52*, 2995.

(28) Wells, H. C.; Haverkamp, R. G. Characterization of the heavy mineral suite in a holocene beach placer, Barrytown, New Zealand. *Minerals* **2020**, *10*, 86.

(29) Ribeiro, J.; Correia, F. C.; Kuzmin, A.; Jonane, I.; Kong, M.; Goñi, A. R.; Reparaz, J. S.; Kalinko, A.; Welter, E.; Tavares, C. Influence of Nb-doping on the local structure and thermoelectric properties of transparent $TiO_2$: Nb thin films. *J. Alloys Compd.* **2020**, *838*, 155561.

(30) Gražulis, S.; Chateigner, D.; Downs, R. T.; Yokochi, A.; Quirós, M.; Lutterotti, L.; Manakova, E.; Butkus, J.; Moeck, P.; Le Bail, A. Crystallography Open Database - an open-access collection of crystal structures. *J. Appl. Crystallogr.* **2009**, *42*, 726−729.

(31) Parker, B. L. I. Zur Kristallographie von Anatas und Rutil. *Z. Kristallogr.-Cryst. Mater.* **1923**, *59*, 1−54.

(32) Meagher, E.; Lager, G. A. Polyhedral thermal expansion in the $TiO_2$ polymorphs; refinement of the crystal structures of rutile and brookite at high temperature. *Can. Mineral.* **1979**, *17*, 77−85.

(33) Verchère, A.; Pailhès, S.; Le Floch, S.; Cottrino, S.; Debord, R.; Fantozzi, G.; Misra, S.; Candolfi, C.; Lenoir, B.; Daniele, S.; Mishra, S. Optimum in the thermoelectric efficiency of nanostructured Nb-doped $TiO_2$ ceramics: from polarons to Nb−Nb dimers. *Phys. Chem. Chem. Phys.* **2020**, *22*, 13008−13016.
(34) Arbiol, J.; Cerdà, J.; Dezanneau, G.; Cirera, A.; Peiró, F.; Cornet, A.; Morante, J. R. Effects of Nb doping on the $TiO_2$ anatase-to-rutile phase transition. *J. Appl. Phys.* **2002**, *92*, 853−861.
(35) Chernet, T. Applied mineralogical studies on Australian sand ilmenite concentrate with special reference to its behaviour in the sulphate process. *Miner. Eng.* **1999**, *12*, 485−495.
(36) Van Deventer, J. Kinetics of the selective chlorination of ilmenite. *Thermochim. Acta* **1988**, *124*, 205−215.
(37) De La Fuente, C.; Marguí, E.; Queralt, I. Niobium-tantalum content of ilmenite-rich black sands from Walikale (North Kivu, Democratic Republic of Congo). *Rev. Soc. Esp. Mineral.* **2010**, *13*, 85−86.
(38) Baba, A. A.; Jacob, S. O.; Olaoluwa, D. T.; Abubakar, A.; Womiloju, A. O.; Olasinde, F. T.; Abdulkareem, A. Y. Processing of a Nigerian columbite-rich ilmenite ore for improved industrial application by sulphuric acid solution. *Indones. Min. J.* **2018**, *21*, 9−19.
(39) Guo, X.; Chen, Y.; Su, M.; Li, D.; Li, G.; Li, C.; Tian, Y.; Hao, C.; Lei, Q. Enhanced Electrorheological Performance of Nb-Doped $TiO_2$ Microspheres Based Suspensions and Their Behavior Characteristics in Low-Frequency Dielectric Spectroscopy. *ACS Appl. Mater. Interfaces* **2015**, *7*, 26624−26632.
(40) Lee, D. Y.; Park, J. H.; Kim, Y. H.; Lee, M. H.; Cho, N. I. Effect of Nb doping on morphology, crystal structure, optical band gap energy of $TiO_2$ thin films. *Curr. Appl. Phys.* **2014**, *14*, 421−427.
(41) Ruiz, A.; Dezanneau, G.; Arbiol, J.; Cornet, A.; Morante, J. R. Study of the influence of Nb content and sintering temperature on $TiO_2$ sensing films. *Thin Solid Films* **2003**, *436*, 90−94.
(42) Karvinen, S. The effects of trace elements on the crystal properties of $TiO_2$. *Solid State Sci.* **2003**, *5*, 811−819.
(43) Buxbaum, G.; Pfaff, G. *Industrial Inorganic Pigments*, 3rd ed.; Wiley-VCH Verlag GmbH, 2005.
(44) Hanaor, D. A. H.; Sorrell, C. C. Review of the anatase to rutile phase transformation. *J. Mater. Sci.* **2011**, *46*, 855−874.
(45) Kong, L.; Wang, C.; Zheng, H.; Zhang, X.; Liu, Y. Defect-Induced Yellow Color in Nb-Doped $TiO_2$ and Its Impact on Visible-Light Photocatalysis. *J. Phys. Chem. C* **2015**, *119*, 16623−16632.
(46) Barksdale, J. *Titanium. Its Occurrence, Chemistry and Technology*; The Ronald Press Company, 1966.
(47) Weiser, P. M.; Zimmermann, C.; Bonkerud, J.; Vines, L.; Monakhov, E. V. Donors and polaronic absorption in rutile $TiO_2$ single crystals. *J. Appl. Phys.* **2020**, *128*, 145701.
(48) Sheppard, L. R.; Bak, T.; Nowotny, J. Electrical properties of niobium-doped titanium dioxide. 3. Thermoelectric power. *J. Phys. Chem. C* **2008**, *112*, 611−617.
(49) Lee, H. Y.; Robertson, J. Doping and compensation in Nb-doped anatase and rutile $TiO_2$. *J. Appl. Phys.* **2013**, *113*, 213706.


https://doi.org/10.1021/acsomega.2c02676
*ACS Omega* 2022, 7, 28258−28264